American Mineralogist, Volume 90, pages 1661–1668, 2005

Mn-tourmaline from island of Elba (Italy): Crystal chemistry

FERDINANDO BOSI,[1,*] GIOVANNA AGROSÌ,[2] SERGIO LUCCHESI,[1] GIOVANNI MELCHIORRE,[2] AND EUGENIO SCANDALE[2]

[1]Dipartimento di Scienze della Terra, Università degli Studi di Roma "La Sapienza", P.le A. Moro 5, 00185 Roma, Italy
[2]Dipartimento Geomineralogico, Università di Bari - Campus, via E. Orabona 4, 70125 Bari, Italy

ABSTRACT

The crystal chemistry of seven crystal fragments taken from differing regions of the same colorless to yellow-greenish tourmaline macro-crystal from pegmatite pockets in aplite veins (island of Elba, Italy) was studied with a multi-disciplinary (SREF, XRDT) and multi-analytical approach (EMPA, SIMS). EMPA and XRDT studies showed relationships between color and chemical zoning and crystal-growth evolution, indicating which fragments could be considered representative of the chemical evolution of the genetic micro-environment in which the crystal developed.

Results showed that the colorless fragment is an elbaite while the yellow-greenish crystal fragments are Mn^{2+}-rich (up to 1.34 apfu) and belong to the alkali group and fluor subgroup. They are characterized by dehydroxylation and alkali-defect type substitutions that cooperate in reducing Li and increasing Mn contents. The Y site is populated by Al, Li, and Mn^{2+}, and the Z site by Al and Mn^{2+} (up to 0.10 apfu). In contrast with data in the literature, Mn^{2+} populates both octahedral sites according to the order-disorder reaction: $^{Y}Mn + {}^{Z}Al \leftrightarrow {}^{Y}Al + {}^{Z}Mn$. As Mn^{2+} content increases, progressive disorder takes place. This disorder is quantitatively lower than that of the ^{Z}Mg in dravite, due to the low structural tolerance of the small Z cavity in the incorporation of larger cations by the $^{Z}R^{2+} \rightarrow {}^{Z}Al$ substitution. Relationships of direct proportionality between lattice parameters and both <Y-O> and <Z-O> are observed. The expansion of both octahedra, as well as of lattice parameters, increases linearly as a function of $^{Y}Mn^{2+}$ and $^{Z}Mn^{2+}$. The latter has greater weight in dictating unit-cell variations, due to the degree of size mismatch between $^{Z}Mn^{2+} \rightarrow {}^{Z}Al$ and $^{Y}Mn^{2+} \rightarrow {}^{Y}Li$ substitutions, and the way in which the Z octahedra are articulated in the structure.

INTRODUCTION

Growth-history reconstruction of minerals from pegmatite pockets in aplite veins (island of Elba, Italy) was carried out with the aim of defining the growth marks, which may characterize the chemico-physical conditions of the growth medium (Graziani et al. 1990). In particular, beryl crystals of various colors and habit developments showed variations in minor element concentrations related to the chemical evolution of the growth medium itself (Scandale et al. 1990). To verify the possibility of general comparison of results with minerals from the same growth environment, tourmalines from pegmatite pockets of the same locality were studied. These tourmalines exhibit color zoning perpendicular to and parallel to **c**: the transition from the inner yellow-greenish regions to the colorless ones occurs suddenly, and minor-element concentration variations are closely related to the observed color zoning.

These results suggested extending study in two different but closely related directions: crystal-chemical characterization and growth-history reconstruction. The latter allowed identification of the various crystal-growth stages, so that fragments representative of the chemical evolution of the genetic micro-environment in which the crystal had developed could be extracted. In this way, substitutional mechanisms could be unequivocally defined, elucidating "...the covariance of structure and chemistry that occurs in portions of a single crystal..." (Hughes et al. 2004). A paper on growth history reconstruction is in progress; the present paper focuses on crystal chemistry.

The general formula of tourmaline is $XY_3Z_6[T_6O_{18}](BO_3)_3V_3W$, where: X = Ca, Na, K, □; Y = Li, Mg, Fe^{2+}, Mn^{2+}, Zn, Al, Cr^{3+}, V^{3+}, Fe^{3+}, Ti^{4+}; Z = Mg, Fe^{2+}, Al, Fe^{3+}, Cr^{3+}, V^{3+}; T = Si, Al, B; B = B, (□); V = OH, O; W = OH, F, O. The complexity of the matrix structure of tourmaline allows great compositional flexibility, associated with partial intracrystalline disorder. The Elba tourmaline has a particularly high MnO content (up to 9.5 wt%) in the yellow-greenish regions, but it drops to below detection limits in the colorless one. Mn-tourmalines have been described since the 20th century, and are nowadays known in a variety of geological settings throughout the world (Shigley et al. 1986 and references therein; Schmetzer and Bank 1984; Novàk 2000). The first structural refinement was carried out by Nuber and Schmetzer (1984), and further crystal-chemical studies include those of Grice and Ercit (1993), Burns et al. (1994), and Ertl et al. (2003, 2004). All papers report complete ordering of Mn at the Y site and full occupancy of Al at the Z: despite this homogeneity in the Z population, the <Z-O> bond distance ranges from 1.902 to 1.910 Å. Some of these Mn-tourmaline crystals are also characterized by significant amounts of Fe, thus posing further

* E-mail: ferdinando.bosi@uniroma1.it

0003-004X/05/0010–1661$05.00/DOI: 10.2138/am.2005.1852

crystal-chemical problems. Our tourmaline crystals allowed us to overcome these difficulties, since they were totally Fe-free.

Experimental methods

Occurrence

The crystals were found in a druse of the aplitic dyke of Grotta d'Oggi, San Piero in Campo (island of Elba, Italy), which crosses the outer portions of the granodioritic massif of Monte Capanne (Marinelli 1959). The dike has an almost homogeneous mineralogical composition, with prevailing quartz, K-feldspar, plagioclase, and schorl, minor biotite, elbaite, and beryl (Carobbi and Rodolico 1976; Orlandi and Scortecci 1985).

The tourmaline crystals are generally elongated $\{10\bar{1}0\}$ and $\{11\bar{2}0\}$ prisms terminating in prominent {0001} pedio and $\{10\bar{1}1\}$ pyramidal faces. The prism faces are frequently striated. These tourmalines are yellow-greenish to colorless, and exhibit color zoning perpendicular to and parallel to **c**.

X-ray topography

A topographic study was carried out on slices about 1 mm thick, cut perpendicular to and parallel to the crystallographic **c** axis. The topograph shown in Figure 1a was taken from a slice cut parallel to the **c** axis and perpendicular to the $[1\bar{2}10]$ direction. Slices were mechanically polished using standard procedures.

X-ray diffraction topographs (XRDT) were made in transmission geometry (Lang 1959) using a C.G.R. camera, and were recorded on Ilford high-resolution plates. Monochromatic radiation (Mo$K\alpha_1$) with a conventional source was used, and the condition $\mu t \approx 1$ (μ = linear absorption coefficient; t = crystal thickness) was satisfied.

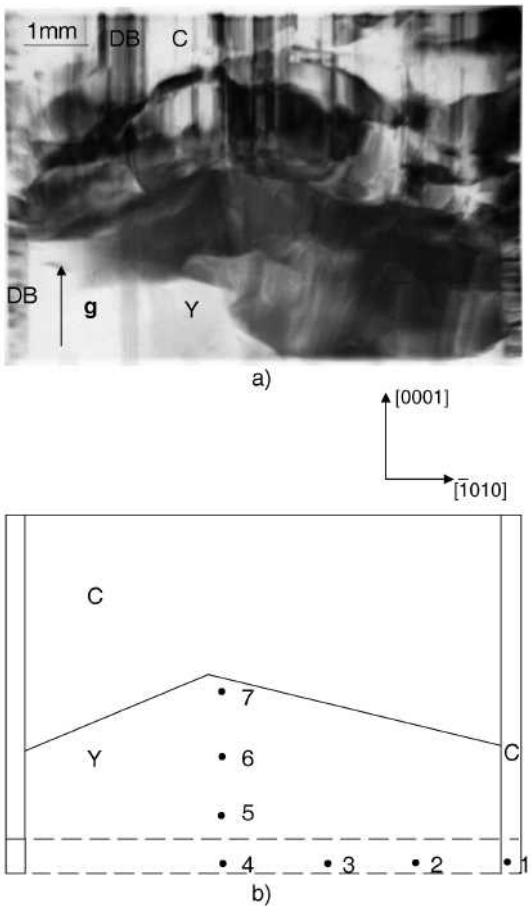

Figure 1. Tourmaline crystal from Elba Island. Slice II2. Y and C: yellow-greenish and colorless regions. (**a**) X-ray diffraction topograph. Diffraction vector **g** = 0003. DB: dislocation bundles perpendicular to $\{10\bar{1}0\}$ and (0001) growing faces. (**b**) Sketch. Dashed line: region from which basal slice was cut. Crystal fragments for SREF are: 1 = Elb2rim, 2 = Tsl2w, 3 = Tsl2m, 4 = Tsl2g, 5 = Tsl2x, 6 = Tsl2z, 7 = Tsl2y.

X-ray diffraction

Structural refinements were performed on seven fragments of approximately prismatic shape (~0.2 mm) extracted from crystal regions considered representative of the various growth stages and the chemical evolution of the genetic microenvironment in which the crystal had developed. Four fragments were taken from rim to core of the basal slice, along the $[\bar{1}010]$ direction: one fragment (Elb2rim) belongs to the colorless region, labeled C, and three (Tsl2w, Tsl2m, Tsl2g) to the yellow-greenish region, labeled Y. Two more fragments (Tsl2x, Tsl2z) were extracted from the yellow-greenish region Y of slice $(1\bar{2}10)$ along the [0001] direction, and one (Tsl2y) at the growth stage boundary between Y and C of the same slice (Fig. 1b).

X-ray data collection was performed with a four-circle Siemens *P*4 automated diffractometer (Table 1). Cell parameters (Table 2) were measured using 52 reflections (13 independent, and their Friedel pairs, on both sides of the direct beam). Scan speed was variable, depending on reflection intensity, estimated with a pre-scan. Background was measured with a stationary crystal and counter at the beginning and end of each scan, in both cases for half the scan time. Preliminary full reciprocal space exploration was accomplished and no violations of *R*3*m* symmetry were noted.

Data reduction was performed with the SHELXTL-PC program. Intensities were corrected for Lorentz and polarization effects. Absorption was accomplished with a semi-empirical method. Only reflections with $I > 2\sigma(I)$ were used from the original set of 3408-3506 data, in a full-matrix least-squares refinement, with unitary weights, in the *R*3*m* space group. Absolute configuration was evaluated according to Barton (1969) and starting coordinates were taken from Foit (1989). Variable parameters were: scale factor, isotropic secondary extinction coefficient, atomic coordinates, site scattering values (expressed as mean atomic numbers, m.a.n.) of X, Y, Z, B, and T sites, and displacement factors (Tables 2, 3, and 4). No chemical constraints were applied during refinement. Scattering curves for 50% ionized Si, Al, and O, fully ionized Mn^{2+}, Li, Na, and F were used, because they furnished the best values of conventional agreement factors over all $\sin\theta/\lambda$ intervals. The boron neutral scattering curve against vacancy at the B site was used, to account

Table 1. Parameters for X-ray data collection

Determination of unit-cell parameters	
Radiation	Mo$K\alpha_1$ (0.70930 Å)
Reflections used	13 (Friedel pairs on both +2θ and –2θ)
Range	85°–95° 2θ
Temperature	296 K
Diffraction intensity collection	
Radiation	Mo$K\alpha$ (0.71073 Å)
Monochromator	High crystallinity graphite crystal
Range	3°-95° 2θ
Reciprocal space range	$0 \le h, k \le 34 \quad -15 \le l \le 15$
Scan method	ω
Scan range	2.4° 2θ
Scan speed	Variable 2.93–29.30° 2θ/min
Temperature	296 K
Data reduction	
Refinement	SHELXTL - PC
Corrections	Lorentz, Polarization
Absorption correction	Semi-empirical, 13 Ψ scans (10°-95° 2θ)

Table 2. Mn-tourmaline from Elba (Italy): crystal and refinement (in *R*3*m* space group) data

Crystal	*a* (Å)	*c* (Å)	*V* (Å^3)	No. refl.	EXT.	R_{obs}(%)	GooF
Elb2rim	15.8232(7)	7.0960(4)	1538.63(16)	3408	27(3)	2.56	1.229
Tsl2y	15.9055(6)	7.1270(3)	1561.46(13)	3473	120(5)	3.23	1.444
Tsl2z	15.9137(6)	7.1302(3)	1563.78(14)	3480	126(6)	3.44	1.518
Tsl2w	15.9243(5)	7.1323(3)	1566.32(12)	3484	239(8)	3.22	1.559
Tsl2x	15.9303(6)	7.1341(3)	1567.90(14)	3492	113(4)	2.96	1.289
Tsl2m	15.9398(6)	7.1363(3)	1570.25(14)	3496	173(7)	3.36	1.438
Tsl2g	15.9461(5)	7.1380(3)	1571.87(12)	3506	98(5)	2.96	1.401

Notes: no. refl. = number of observed independent reflections; EXT. = Isotropic secondary extinction coefficient (×10^5); $R_{obs} = (\Sigma|F_{obs} - F_{calc}|)/(\Sigma F_{obs})$; GooF = goodness of fit.
Refinements carried out up to 70° 2θ gave lower R_{obs} values (from 1.85 to 2.58%): bond-distance and m.a.n. values obtained in both cases are within experimental error.

TABLE 3. Mn-tourmaline: atomic coordinates and anisotropic displacement parameters ($\times 10^4$ Å^2)

Atom		Elb2rim	Tsl2y	Tsl2z	Tsl2w	Tsl2x	Tsl2m	Tsl2g
X	x	0	0	0	0	0	0	0
	y	0	0	0	0	0	0	0
	z	0.23197(22)	0.23267(30)	0.23166(32)	0.23014(31)	0.22918(32)	0.22836(39)	0.22773(36)
	U_{eq}	0.0151(4)	0.0225(6)	0.0233(6)	0.0227(6)	0.0233(6)	0.0236(8)	0.0247(7)
Y	x	0.12281(5)	0.12318(4)	0.12330(4)	0.12349(4)	0.12357(3)	0.12374(4)	0.12394(3)
	y	½ x	½ x	½ x	½ x	½ x	½ x	½ x
	z	0.63493(9)	0.62744(9)	0.62683(9)	0.62602(8)	0.62546(7)	0.62473(8)	0.62407(7)
	U_{eq}	0.0065(2)	0.0083(2)	0.0089(2)	0.0083(1)	0.0095(1)	0.0096(1)	0.0102(1)
Z	x	0.29677(2)	0.29758(3)	0.29771(3)	0.29780(3)	0.29783(2)	0.29795(3)	0.29801(2)
	y	0.26010(2)	0.26086(3)	0.26099(3)	0.26112(3)	0.26115(2)	0.26127(3)	0.26130(2)
	z	0.60947(5)	0.61151(6)	0.61151(7)	0.61148(6)	0.61123(6)	0.61119(7)	0.61129(6)
	U_{eq}	0.00504(8)	0.0051(1)	0.0056(1)	0.0048(1)	0.00522(9)	0.0048(1)	0.00558(9)
B	x	0.10901(5)	0.10969(6)	0.10975(6)	0.10982(6)	0.10984(6)	0.10992(7)	0.11008(6)
	y	2x	2x	2x	2x	2x	2x	2x
	z	0.45411(18)	0.45457(23)	0.45422(25)	0.45407(23)	0.45416(22)	0.45388(25)	0.45402(23)
	U_{eq}	0.0046(3)	0.0050(4)	0.0058(4)	0.0046(4)	0.0058(4)	0.0050(4)	0.0062(4)
T	x	0.19173(2)	0.19192(2)	0.19195(2)	0.19195(2)	0.19187(2)	0.19189(2)	0.19192(2)
	y	0.18971(2)	0.18996(2)	0.18999(2)	0.19000(2)	0.18992(2)	0.18993(2)	0.18993(2)
	z	0	0	0	0	0	0	0
	U_{eq}	0.00431(7)	0.00401(8)	0.00453(9)	0.00377(8)	0.00411(8)	0.00397(9)	0.00456(8)
O1	x	0	0	0	0	0	0	0
	y	0	0	0	0	0	0	0
	z	0.77928(33)	0.78262(46)	0.78207(51)	0.78168(47)	0.78032(43)	0.77963(51)	0.77933(46)
	U_{eq}	0.0315(8)	0.060(1)	0.062(2)	0.062(2)	0.056(1)	0.056(1)	0.060(1)
O2	x	0.06031(4)	0.06091(5)	0.06098(5)	0.06105(5)	0.06116(5)	0.06126(6)	0.06136(5)
	y	2x	2x	2x	2x	2x	2x	2x
	z	0.48895(16)	0.48293(22)	0.48263(24)	0.48194(22)	0.48259(21)	0.48260(25)	0.48263(22)
	U_{eq}	0.0134(3)	0.0192(4)	0.0200(5)	0.0194(4)	0.0204(4)	0.0201(5)	0.0212(4)
O3	x	0.26463(10)	0.26857(11)	0.26871(12)	0.26892(11)	0.26860(10)	0.26871(12)	0.26864(11)
	y	½ x	½ x	½ x	½ x	½ x	½ x	½ x
	z	0.50717(13)	0.50990(17)	0.51005(18)	0.50987(17)	0.50981(16)	0.50975(19)	0.51008(17)
	U_{eq}	0.0121(3)	0.0103(3)	0.0106(4)	0.0099(3)	0.0110(3)	0.0109(4)	0.0117(3)
O4	x	0.09352(4)	0.09335(5)	0.09330(5)	0.09335(5)	0.09346(4)	0.09348(5)	0.09350(4)
	y	2x	2x	2x	2x	2x	2x	2x
	z	0.07346(13)	0.07149(17)	0.07079(18)	0.07076(17)	0.07035(16)	0.06993(18)	0.06984(16)
	U_{eq}	0.0082(2)	0.0075(3)	0.0085(3)	0.0074(3)	0.0082(3)	0.0077(3)	0.0086(3)
O5	x	0.18686(8)	0.18670(10)	0.18656(10)	0.18651(10)	0.18679(9)	0.18684(11)	0.18703(9)
	y	½ x	½ x	½ x	½ x	½ x	½ x	½ x
	z	0.09576(13)	0.09304(17)	0.09286(18)	0.09263(17)	0.09241(16)	0.09184(19)	0.09168(17)
	U_{eq}	0.0086(2)	0.0079(3)	0.0084(3)	0.0079(3)	0.0085(3)	0.0083(3)	0.0090(3)
O6	x	0.19507(4)	0.19695(6)	0.19712(6)	0.19724(6)	0.19719(5)	0.19730(6)	0.19736(6)
	y	0.18476(5)	0.18684(6)	0.18702(6)	0.18712(6)	0.18703(6)	0.18708(7)	0.18720(6)
	z	0.77465(9)	0.77565(11)	0.77570(12)	0.77553(11)	0.77546(11)	0.77557(12)	0.77556(11)
	U_{eq}	0.0064(2)	0.0068(2)	0.0072(2)	0.0066(2)	0.0072(2)	0.0069(2)	0.0079(2)
O7	x	0.28623(4)	0.28554(6)	0.28555(6)	0.28553(6)	0.28555(5)	0.28545(6)	0.28538(5)
	y	0.28591(4)	0.28578(5)	0.28583(6)	0.28579(5)	0.28593(5)	0.28586(6)	0.28584(5)
	z	0.07804(9)	0.08043(11)	0.08029(12)	0.08038(11)	0.07991(11)	0.08000(12)	0.08001(11)
	U_{eq}	0.0056(2)	0.0056(2)	0.0060(2)	0.0054(2)	0.0058(2)	0.0055(2)	0.0064(2)
O8	x	0.20954(4)	0.20989(6)	0.20999(6)	0.20995(6)	0.20995(5)	0.21004(6)	0.21007(6)
	y	0.26996(5)	0.27071(6)	0.27077(7)	0.27074(6)	0.27081(6)	0.27095(7)	0.27096(6)
	z	0.43888(10)	0.44137(12)	0.44151(13)	0.44136(12)	0.44136(12)	0.44127(14)	0.44143(12)
	U_{eq}	0.0064(2)	0.0072(2)	0.0076(2)	0.0069(2)	0.0076(2)	0.0073(2)	0.0081(2)
H3	x	0.2565(27)	0.2664(41)	0.2689(42)	0.2609(29)	0.2611(37)	0.2471(56)	0.2636(50)
	y	½ x	½ x	½ x	½ x	½ x	½ x	½ x
	z	0.3690(64)	0.3818(84)	0.3779(86)	0.3867(57)	0.3870(73)	0.393(11)	0.3865(94)
	U_{eq}	0.05(1)	0.09(2)	0.08(2)	0.03(1)	0.09(2)	0.16(3)	0.13(3)

for ionization effects (Camara et al. 2002). The chosen combination of scattering curves also gave satisfactory agreement (within 1%) between total scattering values obtained by structural refinement and chemical analysis. The occupancies of the Y site were obtained considering the presence of both Al and Mn^{2+}, except for crystal Elb2rim, in which Al vs. Li occupancy was refined. Three cycles with isotropic thermal factors were followed by anisotropic ones until convergence to satisfactory *R* values (from 2.56% to 3.44%, Table 2), which were in good agreement with those expected for tourmaline with data collection up to 95° 2θ (Foit 1989). Mean bond distances, polyhedral volumes, bond-distance distortions (Shannon 1976), quadratic elongations (Robinson et al. 1971), and site m.a.n. are listed in Table 4.

Chemical analysis

After X-ray data collection, the same crystals were mounted on glass slides, polished and carbon coated for electron microprobe analysis (WDS-EDS method) with a CAMECA SX50 electron microprobe, operating at 15 KV and 15 nA (sample current) and with a 5 μm beam. Raw data were reduced using the ZAF program. Natural and synthetic standards were used: wollastonite (Si,Ca), jadeite (Al,Na), magnetite (Fe), periclase (Mg), rutile (Ti), orthoclase (K), rhodonite (Mn), fluorphlogopite (F), and metallic Zn. From 10 to 15 point analyses were performed for each specimen along two orthogonal traverses. The chemical composition data (Table 5) are the average of spot analyses, and their standard deviations account for crystal homogeneity. Each element determination was accepted after checking that the intensity of the analyzed standard before and after each determination was within 1%. Concentrations of Li, B, and H (Table 5) were determined from the same fragments by SIMS (Secondary Ion Mass Spectrometry) using a Cameca IMS 3f at the Centre de Recherches Pétrographiques et Géochimiques (C.N.R.S., Nancy, France). Experimental conditions were: primary current of oxygen negative ions, intensity 5 nA, focused on 10 μm; secondary current of positive ions; voltage offset –60 V; energy window 10 V. Measurements were carried out with an electron multiplier in counting mode and with automatic centering of the magnetic field (Deloule et al. 1992). Beryllium, C, and N were checked to establish whether their contents were significant for possible substitutions at the tourmaline sites. However, the results did not support this conjecture, as the Be content only reached a maximum of 15 ppm, and C and N were practically absent. Details of

TABLE 4. Mn-tourmaline from Elba (Italy): mean bond distances (Å), polyhedral volumes V (Å^3), quadratic elongation <λ>, bond-distance distortion Δ, and m.a.n.

Crystal	Elb2rim	Tsl2y	Tsl2z	Tsl2w	Tsl2x	Tsl2m	Tsl2g
<B-O>	1.374(1)	1.375(1)	1.376(1)	1.376(1)	1.376(1)	1.376(1)	1.376(1)
m.a.n. B	4.81(5)	4.82(6)	4.86(7)	4.74(6)	4.88(6)	4.82(6)	4.86(6)
<T-O>	1.6161(6)	1.6192(7)	1.6195(8)	1.6204(7)	1.6206(7)	1.6203(8)	1.6206(7)
V_T	2.160(1)	2.173(2)	2.174(2)	2.178(2)	2.180(2)	2.179(2)	2.180(2)
$<\lambda_T>$	1.0019	1.0017	1.0017	1.0017	1.0015	1.0014	1.0013
Δ_T	0.00006	0.00006	0.00006	0.00006	0.00005	0.00005	0.00005
m.a.n. T	13.87(4)	14.05(5)	14.08(7)	14.01(5)	14.01(4)	14.07(5)	13.99(5)
<X-O>	2.666(1)	2.674(2)	2.675(2)	2.676(2)	2.682(2)	2.685(2)	2.688(2)
V_X	31.315(8)	31.582(8)	31.66(1)	31.677(8)	31.887(9)	32.01(1)	32.11(1)
Δ_X	0.00303	0.00364	0.00348	0.00330	0.00311	0.00299	0.00288
m.a.n. X	8.50(6)	9.46(9)	9.45(9)	9.68(9)	8.62(7)	8.19(8)	8.18(7)
<Y-O>	1.996(1)	2.035(1)	2.038(1)	2.040(1)	2.039(1)	2.041(1)	2.042(1)
V_Y	10.232(4)	10.825(6)	10.859(3)	10.903(6)	10.873(5)	10.895(6)	10.909(6)
$<\lambda_Y>$	1.0250	1.0265	1.0267	1.0267	1.0271	1.0273	1.0275
Δ_Y	0.00111	0.00102	0.00099	0.00096	0.00092	0.00090	0.00084
m.a.n. Y	9.19(4)	13.69(6)	14.21(7)	14.76(7)	15.55(7)	16.26(9)	16.47(8)
<Z-O>	1.9062(6)	1.9084(8)	1.9086(9)	1.9094(8)	1.9101(8)	1.9108(9)	1.9112(8)
V_Z	9.040(2)	9.088(3)	9.089(3)	9.103(3)	9.111(3)	9.123(3)	9.129(3)
$<\lambda_Z>$	1.0148	1.0136	1.0136	1.0135	1.0136	1.0136	1.0136
Δ_Z	0.00034	0.00046	0.00046	0.00047	0.00046	0.00048	0.00048
m.a.n. Z	13.00(4)	13.09(5)	13.10(5)	13.11(5)	13.15(4)	13.16(5)	13.16(4)
H3-O	0.99(5)	0.91(6)	0.94(6)	0.89(4)	0.88(5)	0.89(7)	0.89(7)

Note: Uncertainty in brackets. Estimated error for mean bond distance is average of standard deviations obtained for single bond distances.

each element calibration may be found in Federico et al. (1998).

The unit formulas of Table 5 were thus calculated on 31 (O, OH, F) assuming all manganese as Mn^{2+} because: (1) the sum of Y + Z + T was slightly higher than 15, but this excess was within experimental uncertainty (~0.1 apfu), calculated according to error propagation. The calculated content of possible Mn^{3+} would have been within error (calculated according to Wood and Virgo 1989); and (2) it furnished a satisfactory agreement between the sum of total site scatterings of cation populations derived by chemical analysis and that obtained by SREF (Table 5).

Determination of ion distribution

Anionic distribution follows the general preference reported by Hawthorne and Henry (1999): the V site (O3) is occupied by OH and the W site (O1) by F, OH, and O^{2-}. When OH + F > 4 apfu, OH in excess is assigned to the O2 site (Hawthorne 1996; Federico et al. 1998).

The cation distribution was obtained by combining structural and chemical data (Bosi and Lucchesi 2004). This approach reproduces observed parameters by optimizing the cation distribution. Differences between observed and calculated parameters were minimized using the function:

$$F(X_i) = \frac{1}{n}\sum_{j=1}^{n}\left(\frac{O_j - C_j(X_i)}{\sigma_j}\right)^2$$

where O_j is the observed quantity, σ_j its standard deviation, X_i variables, i.e., cation fractions at tetrahedral and octahedral sites, and $C_j(X_i)$ the same quantity as O_j calculated by means of X_i parameters. The n O_j quantities taken into account were: mean bond distances (<T-O>, <Y-O>, <Z-O>) and m.a.n. of the T, Y, and Z sites, total atomic proportions given by microprobe analyses, and constraints imposed by crystal chemistry (total charge and T, Y, and Z site populations). As X site was considered to be populated only by Na, K, Ca, and vacancies, it was not included in the minimization procedure.

Mean bond distances were calculated as the linear contribution of each site cation (X_i) multiplied by its specific bond distance (<T-O>$_i$, <Y-O>$_i$, and <Z-O>$_i$):

$$<T\text{-}O>_{calc.} = \Sigma X_i <T\text{-}O>_i$$
$$<Y\text{-}O>_{calc.} = \Sigma X_i <Y\text{-}O>_i$$
$$<Z\text{-}O>_{calc.} = \Sigma X_i <Z\text{-}O>_i$$

As discussed in Bosi et al. (2005), <Y-O>$_i$ and <Z-O>$_i$ were calculated as the sum of the corresponding cation and anionic radii (Table 6). The <T-O>$_i$ used were: <Si-O> = 1.619 (Bosi and Lucchesi 2004), <Al-O> = 1.750, and <B-O> = 1.470 Å (Shannon 1976).

Optimal site assignments were executed with a quadratic program solver. Chemical and structural data were satisfactorily reproduced according to the geometrical model of Bosi and Lucchesi (2004), in which cation radii were also refined. The corresponding site populations are given in Table 7. Comparable site assignments were obtained using the procedure described by Wright et al. (2000).

RESULTS AND DISCUSSION

X-ray topographic observations

Topographs of the studied slices show that color zoning corresponds to the main growth stages: the first matching the Y region and the others the colorless portion C. Growth stage Y is characterized by a defect density lower than that of stages C, in which several dislocation bundles DB, perpendicular to the {10$\bar{1}$0} and {0001} growing faces, nucleated from impurities absorbed at the growth-stage boundaries (Fig. 1a).

Cation radii at octahedral sites

The effective cation radii at the octahedral sites (Table 6) were optimized by a minimization routine that integrated 44 samples belonging to the following series: schorl-dravite-chromdravite (Bosi and Lucchesi 2004; Bosi et al. 2004), elbaite-schorl (Bosi et al. 2005), and Mn-tourmaline (this study). The results gave new cation radius values for $^{VI}Mn^{2+}$ and ^{VI}Li (both different from those of Shannon 1976) and highlight the fact that the ^{Z}Al cation radius is different from that in schorl-dravite-chromdravite. In fact, ^{Z}Al expressed as a specific bond distance, <^{Z}Al-O>, is 1.900 Å in schorl-dravite-chromodravite and 1.907 Å in elbaite-schorl-Mn-tourmaline. The former series is characterized by a higher $^{Z}R^{2+}$ content with respect to the latter. Variations in <^{Z}Al-O> distance for elbaite crystals have already been reported by MacDonald and Hawthorne (1995). In contrast, the ionic radius of ^{Y}Al did not change during the optimization cycles, following the observation of MacDonald and Hawthorne (1995): "...the Y site seems to be exhibiting much more consistent behavior than the Z site...".

TABLE 5. Mn-tourmaline from Elba (Italy): chemical composition (wt%) based on EMPA and SIMS

	Elb2rim	Tsl2y	Tsl2z	Tsl2w	Tsl2x	Tsl2m	Tsl2g
SiO_2	37.2(5)	36.5(4)	37.1(5)	36.2(4)	36.09(5)	36.16(9)	36.1(3)
TiO_2	–	0.27(4)	0.30(5)	0.33(8)	0.32(1)	0.28(7)	0.32(4)
B_2O_3	11.04	10.36	10.69	10.33	10.28	10.22	10.24
Al_2O_3	41.9(3)	37.3(5)	37.6(4)	37.5(4)	37.31(9)	37.2(2)	37.1(5)
FeO	0.2(1)	–	–	–	–	–	–
MnO	0.23(9)	6.6(1)	7.4(1)	8.0(1)	8.5(1)	9.19(7)	9.6(1)
ZnO	–	0.07(5)	0.08(4)	–	–	–	–
CaO	0.74(8)	0.12(2)	0.14(3)	0.17(3)	0.13(3)	0.14(2)	0.09(4)
Na_2O	1.83(6)	2.48(3)	2.48(7)	2.39(9)	2.31(9)	2.1(1)	2.11(7)
K_2O	–	0.04(1)	0.02(1)	0.04(2)	0.02(1)	0.02(1)	0.03(1)
Li_2O	2.04	1.34	1.27	1.10	0.99	0.85	0.81
F	1.03(8)	1.25(8)	1.03(5)	1.04(2)	0.8(1)	0.7(1)	0.79(3)
H_2O	3.47	3.07	3.15	3.11	3.08	2.95	3.09
O=F	–0.43	–0.53	–0.43	–0.44	–0.35	–0.31	–0.33
Sum	99.22	98.94	100.76	99.81	99.46	99.52	100.03
Number of ions calculated on basis of 31 (O, OH, F)							
Si	5.84(7)	5.98(7)	5.98(7)	5.93(6)	5.94(5)	5.97(5)	5.94(7)
Ti^{4+}	–	0.034(5)	0.037(6)	0.04(1)	0.040(1)	0.034(8)	0.040(5)
B	3.0(1)	2.9(1)	3.0(1)	2.9(1)	2.9(1)	2.9(1)	2.9(1)
Al	7.77(8)	7.20(9)	7.14(8)	7.23(8)	7.24(6)	7.23(6)	7.20(9)
Fe^{2+}	0.03(1)	–	–	–	–	–	–
Mn^{2+}	0.03(1)	0.92(2)	1.01(2)	1.11(2)	1.18(2)	1.29(1)	1.34(2)
Zn	–	0.008(6)	0.010(4)	–	–	–	–
Ca	0.13(1)	0.021(4)	0.025(5)	0.029(6)	0.022(4)	0.025(3)	0.016(7)
Na	0.56(2)	0.79(1)	0.78(2)	0.76(3)	0.74(3)	0.69(4)	0.67(2)
K	–	0.008(2)	0.004(2)	0.009(4)	0.003(1)	0.004(3)	0.007(2)
Li	1.29(6)	0.88(7)	0.83(6)	0.72(7)	0.65(7)	0.56(7)	0.54(7)
F	0.51(2)	0.65(4)	0.53(3)	0.54(1)	0.43(6)	0.39(5)	0.41(1)
OH	3.6(2)	3.4(2)	3.4(2)	3.4(2)	3.4(2)	3.3(2)	3.4(2)
Sum OH, F	4.15	4.00	3.91	3.93	3.81	3.64	3.80
Sum T, Y, Z	14.95(13)	15.02(11)	15.00(13)	15.03(12)	15.05(11)	15.09(11)	15.07(13)
e^- chemical*	211.6	227.7	229.2	231.4	232.8	235.0	235.3
e^- SREF†	211.7	227.8	229.7	230.9	232.9	234.8	235.1

Notes: Errors for oxides are standard deviations of repeated analyses on individual crystals. Uncertainty (wt%) for B_2O_3, Li_2O, and H_2O: 0.56, 0.10, and 0.16 respectively. Standard deviation for ions calculated by error propagation.
* Sum of scattering (epfu) of cation populations derived from chemical analysis.
† Sum of refined site-scattering (epfu) derived from SREF.

Chemical composition

According to Hawthorne and Henry's (1999) classification, all examined tourmalines belong to the alkali group and fluor subgroup: the X site is dominated by Na (0.56–0.79 apfu) and the W site shows F as the major component (0.39–0.65 apfu). Moreover, except for Elb2rim, which shows OH at the O2 site, they are characterized by O^{2-} contents that may reach significant values (up to 0.36 apfu). All crystals are Mn-rich (Mn^{2+} 0.92–1.34 apfu), except Elb2rim, which may be classified as elbaite, lying within the elbaite-rossmannite join. Other major cations are Al and Li, and it should be noted that the Mn-tourmaline crystals are completely devoid of Fe. In the Al-Li-Mn diagram (Hawthorne and Henry 1999), the Mn-tourmaline crystals lie in the elbaite-Mn-dravite-Mn-foitite-oxy-Mn-dravite field, so that the main substitutional mechanism may be described by $\square + 7Mn^{2+} + O^{2-} \rightarrow Na^+ + 4.5Li^+ + 2.5Al^{3+} + (OH + F)^-$. This equation ($r^2 = 0.97$) is characterized by two substitutions: dehydroxylation and alkali-defect, both of which cooperate in reducing Li or increasing Mn contents.

Crystal chemistry

B site. SIMS data show B contents stoichiometric within experimental error. B-site m.a.n. values do not support the hypothesis of slight B sub-stoichiometry, because such amounts do not allow unambiguous detection of vacancies (Hawthorne 1996). Furthermore, <B-O> values are within the range obtained by Pieczka (1999) for B in triangular coordination in tourmaline. On the basis of these observations, the B site is considered to be fully populated by B.

TABLE 6. Optimized octahedral ionic radii (Å)

Ion	Y cation radius	Z cation radius	
Ti^{4+}	[0.605]		
Al^{3+}	0.547	0.550*	0.543†
Fe^{2+}	0.778	0.774	
Mn^{2+}	0.809	0.809	
Zn^{2+}	[0.740]		
Li^+	0.751		

Notes: Uncertainty estimated at ca. 0.001 Å. Mean Z-anion radius constant at 1.357 Å for all crystals. Mean Y-anion radius is function of constituent anion radius. Square brackets: Shannon's ionic radii.
* Valid in elbaite–schorl–Mn-tourmaline.
† Valid in schorl–dravite–chromdravite.

X site. Chemical data show that this site contains major Na and also important vacancy contents (up to 0.32 apfu). Besides traces of K, all crystals show Ca as a minor component; the highest value (0.13 apfu) was observed in Elb2rim. X size shows a positive relationship with vacancy ($r^2 = 0.99$) in Mn-tourmaline, but not in Elb2rim. The latter does not follow this trend, because the hydrogen atom next to the O2 position prevents X-polyhedron enlargement when the vacancy content increases (Bosi et al. 2005). All the crystals show a negative correlation between $^X\square$ and Δ_X ($r^2 = 0.83$): the bond-distance distortion decreases with

TABLE 7. Mn-tourmaline from Elba (Italy): final assigned site populations

	Elb2rim	Tsl2y	Tsl2z	Tsl2w	Tsl2x	Tsl2m	Tsl2g
X site							
Ca	0.125	0.021	0.025	0.029	0.022	0.025	0.016
Na	0.558	0.786	0.776	0.758	0.737	0.686	0.673
K	0.000	0.008	0.004	0.009	0.003	0.004	0.007
vacancy	0.317	0.185	0.195	0.204	0.238	0.285	0.304
Y site							
Ti	0.000	0.032	0.034	0.041	0.039	0.041	0.041
Al	1.666	1.265	1.264	1.238	1.304	1.316	1.302
Fe^{2+}	0.041	0.000	0.000	0.000	0.000	0.000	0.000
Mn^{2+}	0.045	0.844	0.911	1.007	1.084	1.196	1.210
Zn	0.000	0.009	0.011	0.000	0.000	0.000	0.000
Li	1.249	0.851	0.781	0.714	0.572	0.447	0.447
Σ Y	3.000	3.000	3.000	3.000	3.000	3.000	3.000
deviation*$_{<Y-O>}$	0.0005	0.0000	0.0000	0.0003	0.0000	0.0004	0.0001
deviation*$_{m.a.n.}$	0.00	0.00	0.01	0.01	0.00	0.16	0.00
Z site							
Al	6.000	5.948	5.935	5.933	5.921	5.901	5.898
Mn^{2+}	0.000	0.052	0.065	0.067	0.079	0.099	0.102
Σ Z	6.000	6.000	6.000	6.000	6.000	6.000	6.000
deviation*$_{<Z-O>}$	0.0003	0.0000	0.0000	0.0002	0.0000	0.0003	0.0001
deviation*$_{m.a.n.}$	0.00	0.01	0.03	0.02	0.01	0.04	0.04
T site							
Si	5.911	5.974	5.923	5.953	5.922	5.981	5.923
Al	0.000	0.020	0.053	0.047	0.076	0.019	0.077
B	0.089	0.006	0.025	0.000	0.002	0.000	0.000
Σ T	6.000	6.000	6.000	6.000	6.000	6.000	6.000
deviation*$_{<T-O>}$	0.0007	0.0001	0.0001	0.0004	0.0000	0.0009	0.0001
deviation*$_{m.a.n.}$	0.00	0.06	0.13	0.02	0.03	0.07	0.00
W site							
O	0.000	0.000	0.087	0.069	0.189	0.360	0.199
OH	0.490	0.352	0.388	0.393	0.382	0.252	0.392
F	0.510	0.648	0.525	0.538	0.429	0.388	0.409
O2 site							
O	2.852	3.000	3.000	3.000	3.000	3.000	3.000
OH	0.148	0.000	0.000	0.000	0.000	0.000	0.000

Notes: For all samples, the V site is fully OH occupied; B content as in Table 5. Atomic frequencies are given to third decimal point for calculation purposes only.
*Deviation is difference, in absolute values, between observed and calculated quantities.

increasing vacancy content.

T site. Silicon is slightly below 6.00 apfu, so the T site requires other cations to achieve full occupancy. The optimized cation distribution shows small amounts of Al and traces of B, consistent with observed <T-O> and m.a.n. values (Table 7).

In the Elba crystals, the average value of the O-T-O angles, 109.449(5)°, suggests that the TO_4 polyhedrons are only slightly distorted. In fact, values for quadratic elongation $<\lambda_T>$, range from 1.0019 to 1.0013, indicating that the tetrahedra deviate slightly from regularity. In general, the distortion of tetrahedra in tourmaline is not great, when compared with that observed in other mineral groups, e.g., in olivine and garnet, in which it ranges from 1.0050 to 1.0150 (Robinson et al. 1971). Moreover, even within the tourmaline isostructural series, the $<\lambda_T>$ values observed in the Elba crystals are quite small. In the literature, $<\lambda_T>$ values range from 1.0050 to 1.0003 in Ca-tourmaline (T72 sample, MacDonald and Hawthorne 1995) and synthetic foitite (Kahlenberg and Veličkov 2000), respectively. In the Elba crystals, $<\lambda_T>$ shows a negative correlation with <X-O> (r^2 = 0.97), which is consistent with Foit's (1989) deduction on the stability of tourmaline. From the inverse proportionality between <X-O> and tetrahedral distortion, Foit inferred that the smaller the X size, the more distorted the tetrahedron: "...substitutions of cations smaller than Na (principally Ca) markedly distort the tetrahedra... tourmaline in which the X-site is fully occupied by Mg is probably metastable".

Octahedral sites. In Mn-tourmaline, Y site is populated by Al, Li, and Mn^{2+} and is characterized by $Mn^{2+} \rightarrow$ Li substitution (r^2 = 0.99). <Y-O> increases linearly with $^{Y}Mn^{2+}$ content (r^2 = 0.79), because $^{Y}Mn^{2+}$ is larger than ^{Y}Al and ^{Y}Li. Quadratic elongation $<\lambda_Y>$ is positively correlated to $^{Y}Mn^{2+}$ and $^{Z}Mn^{2+}$ (r^2 = 0.98 and 0.99, respectively).

The Z site is populated by Al and Mn^{2+} (0.05-0.10 apfu) and is characterized by $^{Z}Mn^{2+} \rightarrow {}^{Z}$Al. Consequently and consistently with Z-m.a.n. data (13.09-13.16), <Z-O> (1.9084-1.9112 Å) depends on $^{Z}Mn^{2+}$ content (Fig. 2). The Mn^{2+} at Z site for Tsl2x, Tsl2m, and Tsl2g fragments is evident from structural data, whereas for Tsl2w, Tsl2z, and Tsl2y it is a result of optimization process. Since all fragments belong to the same macro-crystal, the optimized formulae support the solution of the $^{Z}Mn^{2+}$ content in all crystals.

In contrast with literature data, in which all Mn-tourmaline crystals show a Z site fully occupied by Al and all Mn^{2+} at the Y site, in our crystals Mn^{2+} populates both octahedral sites according to the order-disorder reaction $^{Y}Mn + {}^{Z}Al \leftrightarrow {}^{Y}Al + {}^{Z}Mn$.

Disorder may be defined as the content of divalent cations at the Z site ($^{Z}R^{2+}$). Manganese disorder is positively correlated to total Mn content. Consequently, a positive and progressive relationship exists between $^{Z}Mn^{2+}$ and $^{Y}Mn^{2+}$ (Fig. 3), but this disorder is quantitatively lower than that of ^{Z}Mg in Mg-tourmaline (Marschall et al. 2004; Bosi and Lucchesi 2004 and references therein). The smaller amount of $^{Z}Mn^{2+}$ with respect to ^{Z}Mg is due to the low structural tolerance of the small Z cavity to the incorporation of larger cations by $^{Z}R^{2+} \rightarrow {}^{Z}$Al. In fact, ZO_6 are arranged in a three-dimensional framework and the extent of disorder depends on the ability of this framework to flex and

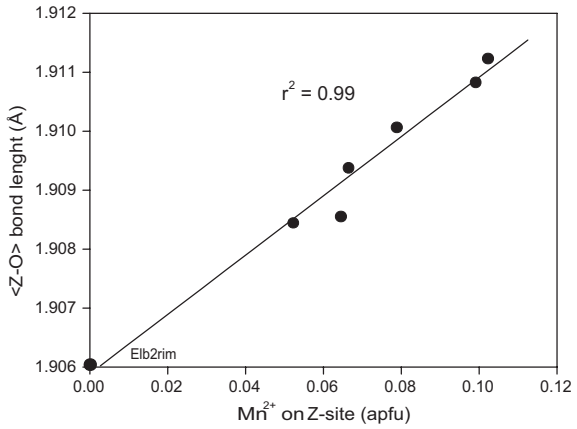

FIGURE 2. Variations of mean <Z-O> bond distance as a function of Mn^{2+} content at Z site.

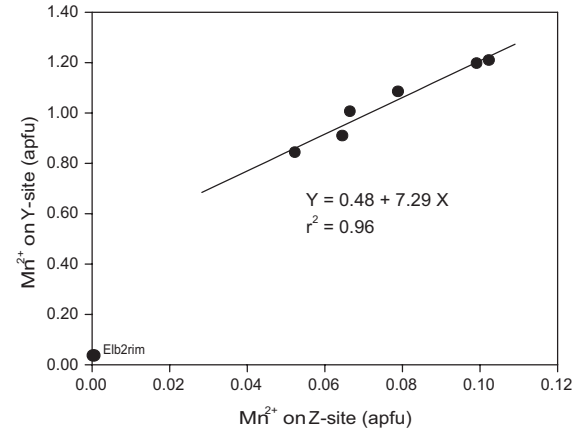

FIGURE 3. Cation distribution of Mn^{2+} at Y and Z sites. Regression line represents progressive disorder of Mn^{2+}, so that $^{Y}Mn^{2+} = 0.48$ when $^{Z}Mn^{2+} = 0$ apfu. Note that Elb2rim is out of alignment.

accommodate differently sized cations. Cation-size mismatch is one of the most important factors controlling the occurrence of cation substitutions at equivalent sites.

Unit-cell parameters. In the literature on tourmaline various attempts have been made to determine the relations between site occupancy and cell dimensions. By multiple linear analysis, Pieczka (2000) correlated the mean bond distances of all polyhedrons with unit-cell parameters. Other authors have tended to use models mainly based on Z and Y sizes (Kargaltsev et al. 1990). In the schorl-dravite series (Bosi and Lucchesi 2004), good correlations were observed between Z size and *c*, Y size and *a*, but not between *a* and *c*. Furthermore, in the Cr-dravite-chromdravite series (Bosi et al. 2004), *a* and *c* are both correlated between themselves and to Z size. In Mn-tourmaline, Ertl et al. (2003) found a positive correlation between *a* and Mn^{2+} at the Y site.

Relationships of direct proportionality between lattice parameters and both Y and Z sizes were observed in our Mn-tourmalines:

$a = 5.9594 \text{ <Y-O>} + 3.7747$ ($r^2 = 0.84$)
$c = 1.5714 \text{ <Y-O>} + 3.9288$ ($r^2 = 0.85$)

$a = 13.1154 \text{ <Z-O>} - 9.1206$ ($r^2 = 0.97$)
$c = 3.3866 \text{ <Z-O>} + 0.6654$ ($r^2 = 0.94$)

The expansion of both octahedra as well as of lattice parameters is consistent with increasing Mn^{2+} content at the octahedral sites:

$$a = 0.1024\ ^{Y}Mn^{2+} + 15.8199 \quad (r^2 = 0.99) \quad (1)$$
$$c = 0.0267\ ^{Y}Mn^{2+} + 7.1052 \quad (r^2 = 0.98) \quad (2)$$
$$a = 0.7459\ ^{Z}Mn^{2+} + 15.8690 \quad (r^2 = 0.94) \quad (3)$$
$$c = 0.1951\ ^{Z}Mn^{2+} + 7.1179 \quad (r^2 = 0.94) \quad (4)$$

As Mn^{2+} content increases, progressive disorder takes place and the unit-cell parameters increase linearly with $^{Z}Mn^{2+}$ and $^{Y}Mn^{2+}$. The slopes of Equations 1, 2, 3, and 4 show that $^{Z}Mn^{2+}$ has greater weight than $^{Y}Mn^{2+}$ in dictating unit-cell variations. This behavior is due both to Z-polyhedron arrangement and to the greater difference in cation radii involved in $^{Z}Mn^{2+} \rightarrow {}^{Z}Al$, with respect to $^{Y}Mn^{2+} \rightarrow {}^{Y}Li$ substitution.

In conclusion, the composition of the minerals of the tourmaline group is quite complex, but the structure is demanding in relation to the relative sizes of the cations at the *Z* sites, with respect to the less rigid Y-polyhedron. The way in which the Z-octahedra articulate clearly affects cell dimensions; in consequence, structural changes are closely related to the progressive disorder of Mn^{2+}, which produces direct proportionality between *a* and *c* ($r^2 = 0.992$).

ACKNOWLEDGMENTS

The authors are grateful to M. Serracino (CNR, IGAG-Rome) who assisted with the EMP analyses, and to G. Walton who revised the English text. This research was supported by a MURST grant, and carried out within the scientific programs of the CNR, IGC-Rome.

REFERENCES CITED

Barton, R. Jr. (1969) Refinement of the crystal structure of buergerite and the absolute orientation of tourmalines. Acta Crystallographica, B25, 1524–1533.
Bosi, F. and Lucchesi, S. (2004) Crystal chemistry of the schorl-dravite series. European Journal of Mineralogy, 16, 335–344.
Bosi, F., Lucchesi, S., and Reznitskii, L. (2004) Crystal chemistry of the dravite-chromdravite series. European Journal of Mineralogy, 16, 345–352.
Bosi, F., Andreozzi, G.B., Federico, M., Graziani, G., and Lucchesi, S. (2005) Crystal chemistry of the elbaite-schorl series. American Mineralogist, 90, in press.
Burns, P.C., MacDonald, D.J., and Hawthorne, F.C. (1994) The crystal chemistry of manganese-bearing elbaite. Canadian Mineralogist, 32, 31–41.
Cámara, F., Ottolini, L., and Hawthorne, F.C. (2002) Crystal chemistry of three tourmalines by SREF, EMPA, and SIMS. American Mineralogist, 87, 1437–1442.
Carobbi, G. and Rodolico, F. (1976) I minerali della Toscana, 280 p. L.S. Olschki, Firenze.
Deloule, E., Chaussidon, M., and Allé, P. (1992) Instrumental limitations for isotope ratio measurements with a Cameca IMS 3f ion microprobe: the example of H, B, S, Sr. Chemical Geology, 101, 187–192.
Ertl, A., Hughes, J.M., Prowatke, S., Rossman, G.R., London, D., and Fritz, E.A. (2003) Mn-rich tourmaline from Austria: structure, chemistry, optical spectra, and relations to synthetic solid solutions. American Mineralogist, 88, 1369–1376.
Ertl, A., Schuster, R., Prowatke, S., Brandstätter, F., Ludwig, T., Bernhardt, H.J., Koller, F., and Hughes, J.M. (2004) Mn-rich tourmaline and fluorapatite in a Variscan pegmatite from Eibenstein an der Thaya, Bohemian massif, Lower Austria. European Journal of Mineralogy, 16, 551–560.
Federico, M., Andreozzi, G.B., Lucchesi, S., Graziani, G., and César-Mendes, J. (1998) Crystal chemistry of tourmalines. I. Chemistry, compositional variations and coupled substitutions in the pegmatite dykes of the Cruzeiro mine, Minas Gerais, Brazil. Canadian Mineralogist, 36, 415–431.
Foit, F.F. Jr. (1989) Crystal chemistry of alkali-deficient schorl and tourmaline structural relationships. American Mineralogist, 74, 422–431.

Graziani, G., Lucchesi, S., and Scandale, E. (1990) General and specific growth marks in pegmatite beryls. Physics and Chemistry of Minerals, 17, 379–384.
Grice, J.D. and Ercit, T.S. (1993) Ordering of Fe and Mg in the tourmaline crystal structure: The correct formula. Neues Jahrbuch Mineralogie Abhandlungend, 165, 245–266.
Hawthorne, F.C. (1996) Structural mechanisms for light-element variations in tourmaline. Canadian Mineralogist, 34, 123–132.
Hawthorne, F.C. and Henry, D. (1999) Classification of the minerals of the tourmaline group. European Journal of Mineralogy, 11, 201–215.
Hughes, J.M., Ertl, A., Dyar, M.D., Grew, E.S., Wiedenbeck, M., and Brandstätter F. (2004) Structural and chemical response to varying $^{[4]}$B content in zoned Fe-bearing olenite from Koralpe, Austria. American Mineralogist, 49, 447–454.
Kahlenberg, V. and Veličkov, B. (2000) Structural investigations on a synthetic alkali-free hydrogen-deficient Fe-tourmaline (foitite). European Journal of Mineralogy, 12, 947–953.
Kargaltsev, S.V., Lebedev, A.S., and Fursenko, D.A. (1990) Relationship of intercation distances and unit cell dimension of tourmaline. Soviet Geology and Geophysics, 31, 105–112.
Lang, A.R. (1959) The projection topograph: a new method in X-ray diffraction microradiography. Acta Crystallografica, 12, 249–250.
MacDonald, D.J. and Hawthorne, F.C. (1995) The crystal chemistry of Si ↔ Al substitution in tourmaline. Canadian Mineralogist, 33, 849–858.
Marinelli, G. (1959) Le intrusioni terziarie dell'Isola d'Elba. Atti Società Toscana di Scienze Naturali, Memorie, 66, 50–253.
Marschall, H.R., Ertl A., Hughes, J.M., and McCammon, C. (2004) Metamorphic Na- and OH-rich disordered dravite with tetrahedral boron associated with omphacite, from Syros, Greece: chemistry and structure. European Journal of Mineralogy, 16, 817–823.
Novàk, M. (2000) Compositional pathways of tourmaline evolution during primary (magmatic) crystallization in complex (Li) pegmatites of the Moldanubicum, Czech Republic. Memorie della Società Italiana di Scienze Naturali e del Museo Civico di Storia naturale di Milano, 30, 45–56.
Nuber, B. and Schmetzer, K. (1984) Structural refinement of tsilaisite (manganese tourmaline). Neues Jahrbuch für Mineralogie Monatshefte, 1984, 301–304.
Orlandi, P. and Scortecci, P.B. (1985) Minerals of the Elba pegmatites. Mineralogical Record, 16, 353–363.
Pieczka, A. (1999) Statistical interpretation of structural parameters of tourmalines: the ordering of ions in the octahedral sites. European Journal of Mineralogy, 11, 243–251.
——— (2000) Modelling of some structural parameters of tourmalines on the basis of their chemical composition. I. Ordered structure model. European Journal of Mineralogy, 12, 589–596.
Robinson, K., Gibbs, G.V., and Ribbe, P.H. (1971) Quadratic elongation: A quantitative measure of distortion in coordination polyhedra. Science, 172, 567–570.
Scandale, E., Lucchesi, S., and Graziani, G. (1990) Growth defects and growth marks in pegmatite beryls. European Journal of Mineralogy, 2, 305–311.
Schmetzer, K. and Bank, H. (1984) Crystal chemistry of tsilaisite (manganese tourmaline) from Zambia. Neues Jahrbuch für Mineralogie Monatshefte, 1984, 61–69.
Shannon, R.D. (1976) Revised effective ionic radii and systematic studies of interatomic distances in halides and chalcogenides. Acta Crystallographica, A32, 751–767.
Shigley, J.E., Kane, R.E., and Manson, D.V. (1986) A notable Mn-rich gem elbaite tourmaline and its relationship to "tsilaisite". American Mineralogist, 71, 1214–1216.
Wood, B.J. and Virgo, D. (1989) Upper mantle oxidation state: ferric iron contents of lherzolite spinels by ^{57}Fe Mössbauer spectroscopy and resultant oxygen fugacity. Geochimica Cosmochimica Acta, 53, 1277–1291.
Wright, S.E., Foley, J.A., and Hughes, J.M. (2000) Optimization of site occupancies in minerals using quadratic programming. American Mineralogist, 85, 524–531.

Manuscript received November 18, 2004
Manuscript accepted February 11, 2005
Manuscript handled by Simona Quartieri